Steel and Composite Structures, *Vol. 33, No. 5 (2019) 729-746*
DOI: https://doi.org/10.12989/scs.2019.33.5.729

Behavior of FRP-reinforced steel plate shear walls with various reinforcement designs

Mehdi Seddighi [1a], Mohammad A. Barkhordari [1b] and S.A.A. Hosseinzadeh[*2]

[1] *Department of Civil Engineering, Faculty of Engineering, Iran University of Science and Technology, Narmak Ave, Tehran, 16846-13114, Iran*
[2] *Department of Civil Engineering, Faculty of Engineering, Golestan University, Al-ghadir Ave, Golestan, 49188-88369, Iran*

(*Received July 8, 2019, Revised October 6, 2019, Accepted November 7, 2019*)

Abstract. The nonlinear behavior of single- and multi-story steel plate shear walls (SPSWs) strengthened with three different patterns of fiber reinforced polymer (FRP) laminates (including single-strip, multi-strip and fully FRP-strengthened models) is studied using the finite element analysis. In the research, the effects of orientation, width, thickness and type (glass or carbon) of FRP sheets as well as the system aspect ratio and height are investigated. Results show that, despite an increase in the system strength using FRP sheets, ductility of reinforced SPSWs is decreased due to the delay in the initiation of yielding in the infill wall, while their initial stiffness does not change significantly. The content/type/reinforcement pattern of FRPs does affect the nonlinear behavior characteristics and also the mode and pattern of failure. In the case of multi-strip and fully FRP-strengthened models, the use of FPR sheets almost along the direction of the infill wall tension fields can maximize the effectiveness of reinforcement. In the case of single-strip pattern, the effectiveness of reinforcement is decreased for larger aspect ratios. Moreover, a relatively simplified and approximate theoretical procedure for estimating the strength of SPSWs reinforced with different patterns of FRP laminates is presented and compared with the analytical results.

Keywords: composite steel plate shear walls; FRP; reinforcement pattern; ultimate strength; initial stiffness; ductility; energy dissipation

1. Introduction

Steel plate shear walls (SPSWs) have been recently proposed as one of the most efficient systems capable of resisting against both wind and earthquake lateral loads. In recent applications, typical SPSWs consist of thin unstiffened steel plates connected to the surrounding horizontal and vertical boundary elements (HBEs and VBEs). Numerical and experimental research works have accepted the high strength, stiffness, and ductility as well as energy dissipation and robustness of various types of this system under pushover/ cyclic loading (Driver *et al*. 1998, Lubell *et al*. 2000, Memarzadeh *et al*. 2010, Vatansever and Yardimci 2011, Chatterjee *et al*. 2015, Kalali *et al*. 2015, Vatansever and Berman 2015, Rahmzadeh *et al*. 2016, Dhar and Bhowmick 2016, Shekastehband *et al*. 2017, Ali *et al*. 2018, Massumi *et al*. 2018, Farzampour *et al*. 2018, Liu *et al*. 2018, Bagherinejad and Haghollahi 2018, Barua and Bhowmick 2019, Deng *et al*. 2019). However, some obstacles, such as the lack of understanding of the behavioral characteristics of this system, still exist that may impede more widespread acceptance of SPSWs. To overcome these impediments and expand the applicability of SPSWs, more study is required regarding the different aspects of the behavior of SPSWs and more research is necessary on various types or configurations of this system that can be used in various practical applications. Also, more research work needs to be done on novel methods or techniques for further improving the performance and effectiveness of this system.

In recent decades, the use of fiber reinforced polymer (FRP) composites for both new and retrofit building constructions has increased considerably. Compared with traditional methods, the use of FRP sheets causes minimum disruption to the function of the buildings and its occupants during retrofitting. They can also be easily and quickly deployed with minimum on-site work necessary. High strength/stiffness to weight ratio and corrosion resistant properties are other distinct advantages of FRP composites. Given the abovementioned advantages and widespread applications, the idea of using FRP laminates for strengthening SPSWs has been recently proposed and studied by very few researchers.

Hatami *et al*. (2012, 2014) numerically and experimentally investigated the effect of carbon fiber reinforced polymer (CFRP) laminates on the improvement of nonlinear behavior of single-story SPSWs (with conventional and low-yield-point (LYP) steel plates). They examined the effect of FRP orientation angle and infill plate width on the behavior of the system. Khazaei-Poul and Nateghi-Alahi (2012) studied nonlinear behavior of SPSW reinforced with FRP laminates based on frame-composite plate interaction. Khazaei-Poul *et al*. (Khazaei-Poul and Nateghi-Alahi 2012, Khazaei-Poul *et al*. 2016) also

∗Corresponding author, Assistant Professor,
E-mail: ahosseinzade@gmail.com; ahosseinzade@gu.ac.ir
[a] Ph.D. Student, E-mail: mehdiseddighi@civileng.iust.ac.ir
[b] Professor, E-mail: barkhordar@iust.ac.ir

http://www.techno-press.org/?journal=scs&subpage=6
ISSN: 1229-9367 (Print), 1598-6233 (Online)

experimentally investigated the effect of number and orientation of FRP layers (glass or carbon) on the behavior of composite steel plate shear walls (CSPSWs) reinforced with fibers. The obtained results demonstrated that the fiber orientation plays a major role in the strength and stiffness of CSPSWs. The behavior and design of steel-frame structures strengthened with glass fiber reinforced polymers (GFRPs)-infill panels (GIPs) was studied by Kwon *et al*. (2015). The reported test results confirmed the improved behavior of the retrofitted system and the proposed design procedure as well. Sahebjam and Showkati (2016) conducted experimental cyclic tests on four CFRP strengthened/non-strengthened perforated SPSWs. The specimens consisted of single-story/single–bay steel frames with a regular staggered pattern of circular openings on the infill plate. Results showed that the fibers direction is the more effective factor on the behavior of composite SPSWs and that reinforcing infill plate with CFRP delays the yielding of the infill plate. They also found that the optimum direction for the fibers is along the tension field. However, strengthening of infill plates with FRP causes the tension field to be tangibly oriented toward the fibers direction. The performance of pristine and retrofitted composite FRP/steel plate shear walls tested and compared by Petkune *et al*. (2016). The test results showed that the retrofitted specimens had higher stiffness, higher ultimate loading capacity and similar energy dissipation capability relative to pristine specimens. Petkune *et al.* (2018) also performed experimental works to study the behavior of steel, pure FRP and hybrid shear walls under cyclic loading concerning stiffness degradation and energy absorption. Based on the obtained results, the researchers expressed that the innovative shear walls with FRP and hybrid infill plates offer excellent load carrying capacity and energy absorption, relatively small loss of stiffness and potential for increased durability in comparison with conventional SPSW systems. Dakhel *et al*. (2019) investigated on the behavior of connections between the composite steel/FRP infill plate and the fish plate of the surrounding frame elements in shear wall systems. The researchers provided a detailed comparison between the specimens having different connection details in aspects of energy absorption, load capacity and modes of failure.

According to the literature review, previous experimental and numerical studies on this topic have only focused on examining the behavior of single-story SPSWs strengthened mainly with a certain type/content of FRP and no research work on the behavior of multi-story SPSWs that can be completely different from the single-story ones (Hosseinzadeh and Tehranizadeh 2014a, b) is available. Moreover, the primary concern of previous studies has been paid to the use of fibers on the whole surface of the infill wall and less attention has been given to the issues of partially reinforcing the infill wall with fibers and various patterns of reinforcement that may be practically used.

In the present paper, the effectiveness of three different reinforcement patterns of FRP (including single-strip (CD pattern), multi-strip (CP pattern) and fully (CS pattern) FRP strengthened models) on the improvement of the behavioral characteristics of composite SPSWs is investigated. To accomplish this, a series of nonlinear static and quasi-static cyclic analyses on a number of single- and multi-story SPSWs strengthened with the different patterns of FRP laminates mentioned above are analyzed using the finite element method, and the obtained results are utilized to investigate the effects of geometrical properties of the system (i.e., (a) aspect ratio; and (b) number of story), as well as the changes in the geometrical and mechanical properties of reinforcement fibers (i.e., (c) the reinforcement pattern; (d) type (material), (e) content (thickness, width or number of layer), and (f) orientation angle) on various aspects of the nonlinear behavior (strength, initial stiffness and ductility) and energy dissipation of the strengthened SPSWs. In the study, the composite wall-frame interaction and the pattern and mode of failure for SPSWs strengthened with the different patterns of fibers are also discussed. Moreover, a relatively simplified and approximate theoretical procedure for estimating the strength of SPSWs reinforced by different patterns of FRP laminates is presented and compared with the analytical results.

2. Method of the stud

2.1 Models

In this research, a number of unreinforced/reinforced single- and multi-story SPSWs with the three different patterns of FRPs mentioned above are considered. Fig. 1 shows the original (unreinforced) SPSW (S) and those reinforced with the different reinforcement patterns considered in the study (including single-strip (CD), multi-strip (CP) and fully (CS) FRP reinforced models).

The original unreinforced models were adopted from Ref. (Hosseinzadeh and Tehranizadeh 2012). For convenience, the design details of these SPSWs are listed in Table 1. Table 2 shows the details of the reduced beam section (RBS) connection for different HBE profiles according to AISC 358-05 (2005). SPSWs were designed according to the capacity design recommendations given in AISC Seismic Provisions (ANSI/AISC 341-05 2005) and AISC Design Guide 20 (Steel Design Guide 20 2007). To ensure concentration of plastic deformation at the desired locations and to limit the bending moment demand to VBEs, RBS connection details were utilized at both ends of HBEs.

For a comprehensive study on the behavior of FRP-strengthened SPSWs, the following geometrical and mechanical parameters are considered in this research work. Note that throughout this article, each SPSW model will be identified by the value of these parameters as well.

- Fiber orientation (θ_f): To investigate the effect of fiber orientation in the CP and CS patterns, the orientation angle of FRPs from the horizontal is considered to vary between 0 (horizontal), 15, 30, 45, 60 and 90° (vertical) (see Fig. 1). It is noteworthy that in the CD pattern, fibers are oriented diagonally and therefore, the orientation (θ_f) is constant for a SPSW with a certain aspect ratio.

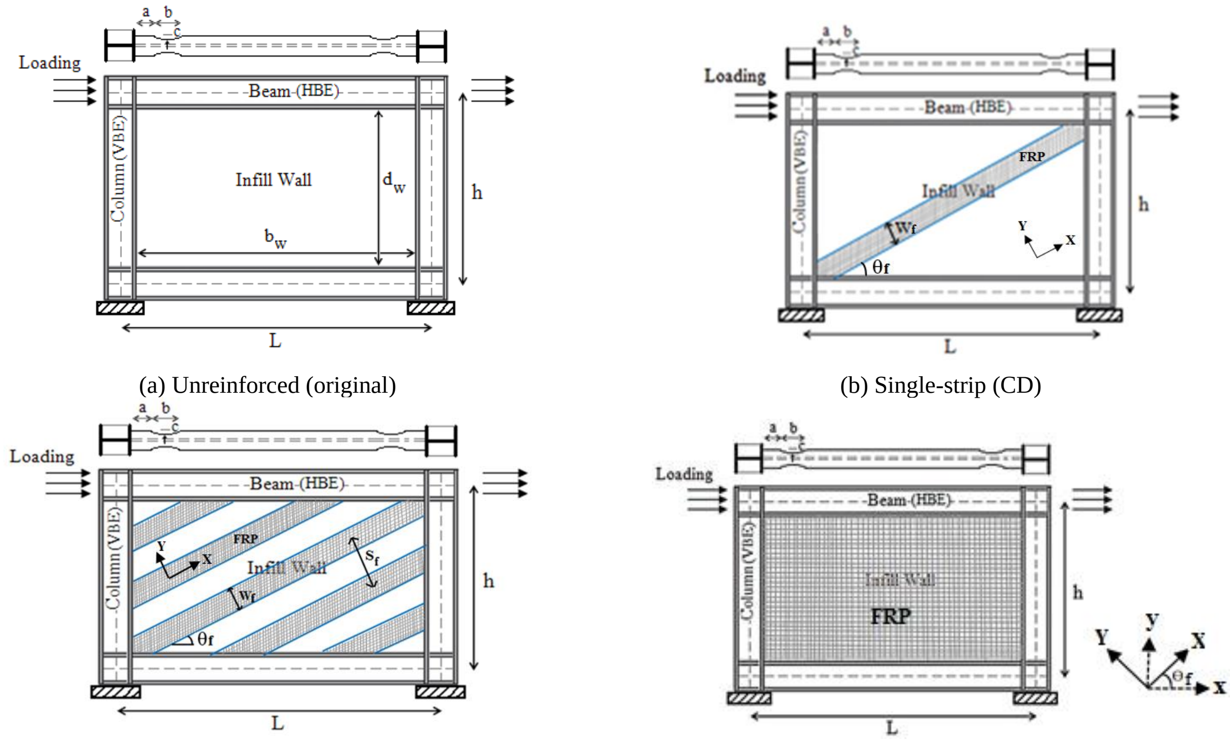

(a) Unreinforced (original)
(b) Single-strip (CD)
(c) Multi-strip (CP)
(d) Fully reinforced (CS)

Fig. 1 Typical single-story SPSW and CSPSW systems with different reinforcement patterns

Table 1 Infill plate thicknesses and frame member sizes at different stories of original SPSWs, adopted from (Hosseinzadeh and Tehranizadeh 2012)

Name	# of stories, n	Bay width, L (m)	Aspect ratio, L/h	Plate thickness, t_w (mm)	HBE size		VBE size
					Intermediate	Base and top	
1S3	1	3	0.86	1st: 3.18	-	W14×176	W14×283
1S4	1	4	1.14	1st: 3.18	-	W14×193	W14×311
1S5	1	5	1.43	1st: 3.18	-	W14×233	W14×370
1S6	1	6	1.71	1st: 3.18	-	W24×250	W14×455
1S7	1	7	2	1st: 3.18	-	W24×370	W14×550
2S5	2	5	1.43	1st,2nd: 3.18	W14×132	W14×233	W14×370
3S5	3	5	1.43	1st~3rd: 3.18	W14×132	W14×233	W14×370
4S5	4	5	1.43	1st~4th: 3.18	W14×132	W14×233	W14×370
6S5	6	5	1.43	1st~4th: 4.76 5st , 6th: 3.18	W14×132	W14×233	1st~4th: W14×500 5st , 6th: W14×370
8S5	8	5	1.43	1st~4th: 6.35 5st , 6th: 4.76 7st , 8th: 3.18	W14×132	W14×233	1st~4th: W14×730 5st~8th: W14×398

Table 2 RBS connection dimensions for different HBE profiles per AISC 358-05 (2005)

RBS dimensions	W14×132	W14×176	W14×193	W14×233	W24×250	W24×370
a (mm)	200	200	200	220	200	175
b (mm)	300	300	300	330	550	600
c (mm)	90	95	95	100	80	85

- Fiber content (A_F/A_w): The fiber content is expressed as the ratio of the total surface area of FRP layers to the total surface area of the infill wall. The total surface area of FRPs is obtained by multiplying the surface area of the infill wall covered by the fibers by the total number of fiber layers (n_f) used on both sides of the wall. Thus, the fiber content can be changed through a change in the number (or total thickness, t_f) of fiber layers in all the reinforcement patterns and/or the width (w_f) of reinforcement strips in the CP and CD patterns.

The total thickness of FRPs (t_f) used on the infill wall surface is considered to vary from 0.5 to 32 mm (so that $A_F/A_w = 1 \sim 8$) in different reinforcement patterns (see Fig. 1). Moreover, the width of fiber strips (w_f) in the CD and CP patterns is assumed to range from 70 to 700 mm (so that $A_F/A_w = 1 \sim 4$). Accordingly, the ratio of the strip width (w_f) to the center-to-center distance of strips (s_f) varies from 0.1 to 1 in the CP pattern, considering that the center-to-center distance of strips (s_f) is assumed to be 700 mm. Preliminary studies have confirmed that the center-to-center distance of strips (s_f) in this pattern does not influence the results at a constant w_f/s_f.

- Type/mechanical properties of fibers: The fiber material for most parts of the work is assumed to be glass fiber (type G1). To investigate the effect of the type/mechanical properties of FRP laminates, other fiber materials including another type of glass fiber (type G2) and a type of carbon fiber (type C) are also considered, but unless otherwise stated, the default fiber material is G1. The properties of the considered FRP materials are presented in Table 3. Based on specifications provided by the manufacturers, the total thickness of a single layar of laminate including fiber strands and adhesive (plastic resin) sheet is almost equal to 0.5, 1 and 0.4 mm in the fiber types of G1, G2 and C, respectively.
- Aspect ratio (L/h): A default story height (h) of 3.5 m, measured from center to center of HBEs, with a bay width (L) of 5 m, measured from center to center of VBEs, are considered for the models in this research (i.e., default ratio of $L/h = 1.43$). However, to investigate the effect of the aspect ratio, the bay widths (L) are assumed to vary from 3 to 7 m (i.e., $L/h = 0.86, 1.14, 1.43, 1.71$ and 2.00).
- Number of story (n): In addition to single-story systems, 2, 3, 4, 6 and 8-story SPSWs are also considered to investigate the effect of the total height.

Table 4 briefly summarizes the values considered in parametric studies for different reinforcement patterns and various SPSW models.

2.2 Mechanical properties of materials

The ASTM-A572 (yield stress: 385 MPa) and ASTM-A36 (yield stress: 327.6 MPa) conventional structural steel standards are, respectively, selected for frame member (i.e., VBEs and HBEs) and infill wall materials. The modulus of elasticity and Poisson's ratio of the both steel materials are considered to be 200 GPa and 0.3, respectively. To study the

Table 3 Mechanical properties of various FRP laminates used in this study

FRP label	Type of FRP	Tensile modulus (GPa)		Tensile strength (MPa)		Tensile elongation (%)
		Longitudinal ($\boldsymbol{E_{xf}}$)	Transverse ($\boldsymbol{E_{yf}}$)	Longitudinal ($\boldsymbol{X^T}$)	Transverse ($\boldsymbol{Y^T}$)	
C	Carbon,SikaWrap®Hex230C	65.40	5.88	894	27	1.33
G1*	Glass,SikaWrap®Hex430G	26.49	7.07	537	23	2.21
G2	Glass,SikaWrap®Hex100G	26.12	6.65	612	30	2.45

* G1: Default fiber material in the study

Table 4 Summary of the values considered in parametric studies for different reinforcement patterns

Rein. pattern	Parameters							
	Fiber						SPSW	
	Orientation, θ_f (°)	Width, W_f (mm)	W_f/S_f	Thickness, t_f (mm)	Content, A_f/A_w	Type	Aspect ratio, L/h	# of Stories, n
CD	-	70, 140, 210, …, 700	-	4, 8, 12, 16, 24, 32	0, 0.4, 0.8, …, 8	C, G1, G2	0.86, 1.14, 1.43, 1.71, 2	1, 2, 3, 4, 6, 8
CP	0, 15, 30, 45, 60, 75, 90	70, 140, 210, …, 700	0.1, 0.2, 0.3, …, 1.0	1, 2, 3, 4, 6, 8	0, 0.4, 0.8, …, 8	C, G1, G2	0.86, 1.14, 1.43, 1.71, 2	1, 2, 3, 4, 6, 8
CS	0, 15, 30, 45, 60, 75, 90	-	-	0.5, 1, 1.5, 2, 3, 4	0, 0.4, 0.8, …, 8	C, G1, G2	0.86, 1.14, 1.43, 1.71, 2	1, 2, 3, 4, 6, 8

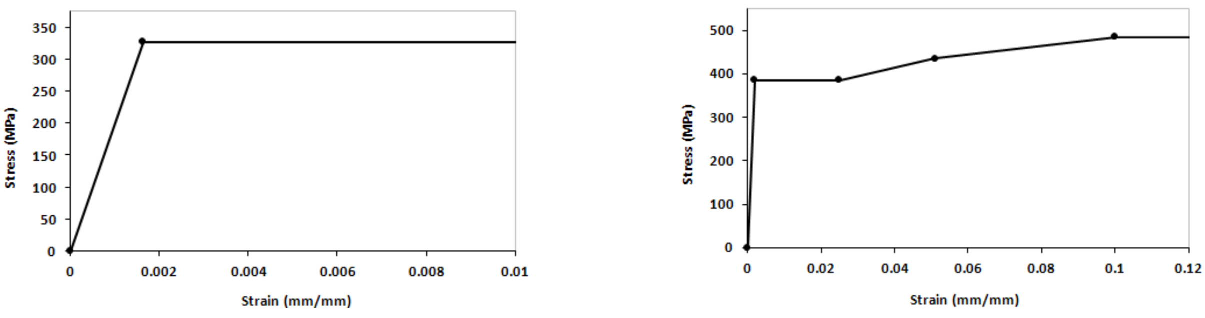

Fig. 2 Material stress-strain curves: (a) infill walls; and (b) frame members (VBEs and HBEs), Adopted from (Habashi and Alinia 2010)

Table 5 Mechanical properties of the selected FRP materials for modeling fracture of FRP

Type	Strength (MPa)						Fracture energy (N/mm)			
	Longitudinal			Transverse			Longitudinal		Transverse	
	Tensile, X^T	Comp., X^C	Shear, S^L	Tensile, Y^T	Comp., Y^C	Shear, S^T	Tensile, G_X^T	Comp., G_X^C	Tensile, G_Y^T	Comp., G_Y^C
C	894	779	63	27	135	63	100	100	0.23	0.46
G1*	537	496	50	23	115	50	200	200	0.23	0.46
G2	612	597	40	30	150	40	200	200	0.23	0.46

* G1: Default fiber material in the study

nonlinear behaviors of frame members and infill walls, respective stress-strain diagrams (Habashi and Alinia 2010) that define the constitutive behaviors of the two steel materials are presented in Fig. 2.

For all incremental pushover analyses, a nonlinear isotropic hardening rule, which is suitable for this type of analysis, is utilized. For quasi-static cyclic analyses that involve a significant number of stress and strain reversals, the Bauschinger effect becomes potentially important. Hence, for this loading case, a kinematic hardening model is applied.

Moreover, as mentioned before, three fiber materials including two types of glass fibers, G1 (the default fiber) and G2, and a type of carbon fiber, C, with the specifications presented in Table 3, are considered for the reinforcement of SPSWs in the study. The FRP laminates are assumed to behave linearly until failure (Nateghi-Alahi and Khazaei-Poul 2012). To take into account longitudinal, transverse and shear failure modes of FRPS, the initiation and propagation of damage in FRPs are implemented in the modeling by Hashin failure criterion (Tabrizi and Rahai 2011, ABAQUS 2014). The values of the various parameters considered for this criterion are presented in Table 5.

2.3 Numerical modeling and method of analysis

The commercial finite element software package, ABAQUS (2014), is used to analysis both linear (buckling) and nonlinear (pushover and cyclic) finite element analyses. All the infill walls, boundary frame members and FRP laminates are modeled with a reasonably fine mesh using the four-noded S4R element, a general purpose shell with reduced integration capable of modeling elastic, plastic and large-strain behaviors. The implicit approach is utilized for all Eigen-value and incremental nonlinear pushover analyses, while due to highly nonlinear nature of the problem and serious convergence difficulties in implicit analysis, the explicit approach is adopted for quasi-static cyclic analyses.

Displacements of all nodes at the bottom of flanges and webs of VBEs in all directions are restrained to replicate the fixed support conditions at the VBE bases. To simulate the effects of the concrete slab of the floors, all HBE webs are also fixed against displacement in the out-of-plane direction. The tie-constraint surface-to-surface contact interaction (ABAQUS 2014) is used to represent the surface contact between the fibers and the infill wall.

The effects of geometric nonlinearity phenomenon are also included in nonlinear analyses as a result of large displacements with small strains. To help precipitate the global buckling and development tension fields in the infill wall, the effect of initial imperfections in the infill wall should also be considered. In the case of unreinforced SPSW models, the choice of imperfection amplitude and shape does not affect the overall behavior of the system significantly, as the infill walls buckle almost at the onset of applied loading (Brando and De Matteis 2011). However, in the case of FRP reinforced SPSW models, preliminary studies by the authors have shown that large magnitudes of initial deformations may have some effects on the behavior of the system. As a result, an initial imperfection pattern consistent with the first buckling mode of the infill wall (Hosseinzadeh and Tehranizadeh 2014b) with a sufficiently

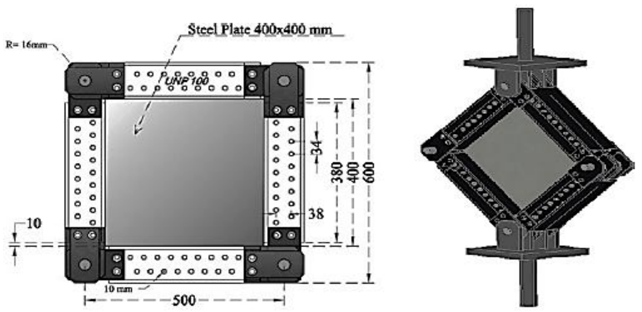

Fig. 3 Details of the specimen (unit: mm) considered for the validation (Nateghi-Alahi and Khazaei-Poul 2012)

small peak magnitude (i.e., 1 mm) is applied in both reinforced/unreinforced SPSW models. The ultimate lateral displacement limit is considered to occur at a drift ratio of 2.5% at least at one of the stories of the models per ASCE 7-05 (2005). In the case of pushover analyses, lateral loads, as shown in Fig. 1, are equally applied to the beam-to-column connections at each story level and are gradually increased from zero to a magnitude beyond the system shear capacity, while in the case of cyclic analyses, the models are loaded at the top based on the displacement controlled scheme and the displacement at that level is considered as the control parameter.

2.4 Validation and verification of results

The finite element (FE) modeling approach's adequacy for representing the pushover/cyclic responses of (unreinforced) SPSWs was previously validated (Hosseinzadeh and Tehranizadeh 2012) by comparing the reported experimental results of Driver's four-story (Driver *et al*. 1998) and Lubell's single-story (only specimen SPSW2) (Lubell *et al*. 2000) specimens with the corresponding FE analysis results, so is not repeated here. To further validate the results of pushover and cyclic analyses for composite SPSWs, the GFRP-reinforced SPSW specimen tested by Nateghi-Alahi and Khazaei-Poul (2012) is modeled and analyzed according to the method explained in the previous section and the specifications mentioned in (Nateghi-Alahi and Khazaei-Poul 2012). Geometric details of the experimental specimen under study

Table 6 Summary of the results of ultimate strength, initial stiffness and ductility of different unreinforced SPSWs (Hosseinzadeh and Tehranizadeh 2012)

Name	Ultimate strength, (KN)			Initial stiffness, (KN/mm)	Ductility
	SPSW	Infill	Frame		
1S3	4746	1425	3321	292.4	6.29
1S4	5597	1960	3637	373.3	6.82
1S5	6885	2505	4380	465.4	6.97
1S6	9587	3050	6537	595.1	6.38
1S7	12632	3544	9088	735.7	6.02
2S5	6602	2501	4101	271.0	7.87
3S5	6185	2509	3676	178.0	7.00
4S5	5617	2519	3098	122.1	5.84
6S5	7328	3408	3920	86.8	4.43
8S5	8744	4597	4147	65.5	3.51

are shown in Fig. 3. Comparisons of experimental cyclic results and those obtained by numerical pushover/cyclic analyses are given in Fig. 4 and reasonable agreement is observed. In addition, the rupture in the fibers and the resulting capacity reduction observed in the experiment are successfully predicted by the FE model that involved Hashin failure criterion (ABAQUS 2014).

3. Discussion of results

In this section, the effectiveness of the considered fiber einforcement patterns (including single-strip (CD pattern), multi-strip (CP pattern) and fully (CS pattern) FRP strengthened models, as described in Fig. 1) in strengthening of SPSWs is studied by comparing the behavior of reinforced and corresponding unreinforced SPSWs in terms of strength, initial stiffness, ductility, and energy dissipation.

After a brief discussion of wall-frame interaction in reinforced and unreinforced SPSWs, the effectiveness of the three reinforcement patterns is examined regarding the reinforcement material and geometrical properties (i.e., fiber orientation, content and material type). Then, the

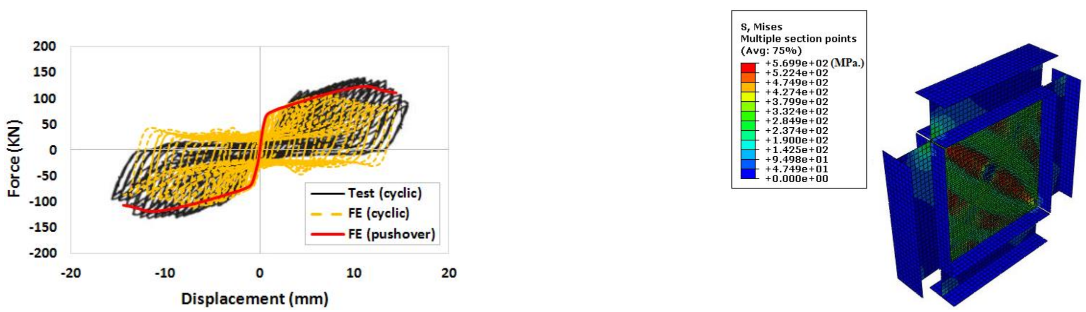

(a) Comparison of numerical analysis results with experimental results (CSPSP3 specimen)

(b) Mises stress of FE model of CSPSP3 specimen at the ultimate state

Fig. 4 Validation of FE model

effects of the system aspect ratio and height on the degree of effectiveness of the different reinforcement patterns are studied. Following this, the effectiveness of the different reinforcement patterns on the improvement of the energy absorption behavior of some single- and multi-story SPSWs are investigated using cyclic analysis results.

A summary of the results of unreinforced SPSW models is presented in Table 6. It is noteworthy that in the next sections, the strength, initial stiffness, and ductility of reinforced models are given in dimensionless form by dividing them by the respective values of the corresponding unreinforced models.

3.1 Wall-frame interactive behavior

Fig. 5 compares the load-displacement diagrams for the infill wall, frame and the overall system of a typical single-story unreinforced SPSW ($L/h = 1.43$) and those of the reinforced with different reinforcement patterns but the same content ($A_F/A_W = 2$).

Figs. 5(a) and (c) shows that for an assumed FRP content, the nonlinear behavior of the composite infill wall and the load-bearing capacity of the system can vary, depending on the reinforcement pattern of FRP. The reinforcement pattern of FRP does effect on the mode of failure and occurrence of rupture in the fiber as well. The results in Fig. 5(b) indicate that the behavior of the frame of unreinforced SPSW may be somewhat different from that of the corresponding composite system, due to the increased interaction effect between composite-wall and frame as compared with that of the unreinforced SPSW. Similar results were observed for SPSW frame and bare frame in the recent work by the author (Hosseinzadeh and Tehranizadeh 2014b). Fig. 5(c) also shows that the use of FRP laminates improves the overall behavior of SPSWs to some extent, depending on the content and pattern of reinforcement.

Fig. 6 presents the von Mises stress distribution in typical single-story unreinforced and FRP-reinforced SPSWs ($L/h = 1.43$ and $A_F/A_W = 2$) at the ultimate state (at drift ratio of 2.5% or at the time of FRP rupture, as can be shown in Fig. 5). As can be seen, the stress distributions in all reinforced and unreinforced SPSWs are almost similar, where yield zones spread throughout the infill walls and plastic hinges are formed at the VBE bases and both ends of HBEs. However, the maximum stress observed in the SPSW frame is slightly greater for the reinforced models due to an increase in the forces imposed by the reinforced infill wall to the frame members.

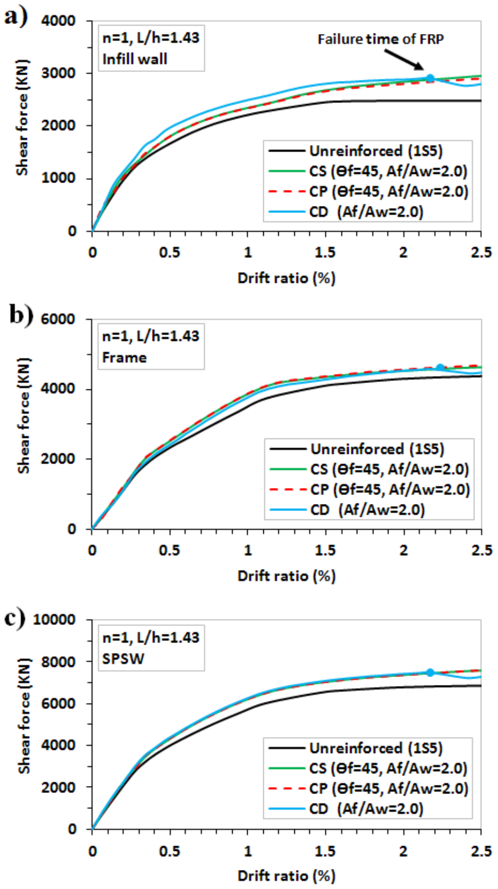

Fig. 5 Comparisons of shear force-drift ratio curves of (a) infill wall; (b) frame; and (c) total system, for unreinforced and reinforced SPSWs for the reinforcement patterns of CD, CP ($\theta_f = 45°$) and CS ($\theta_f = 45°$)

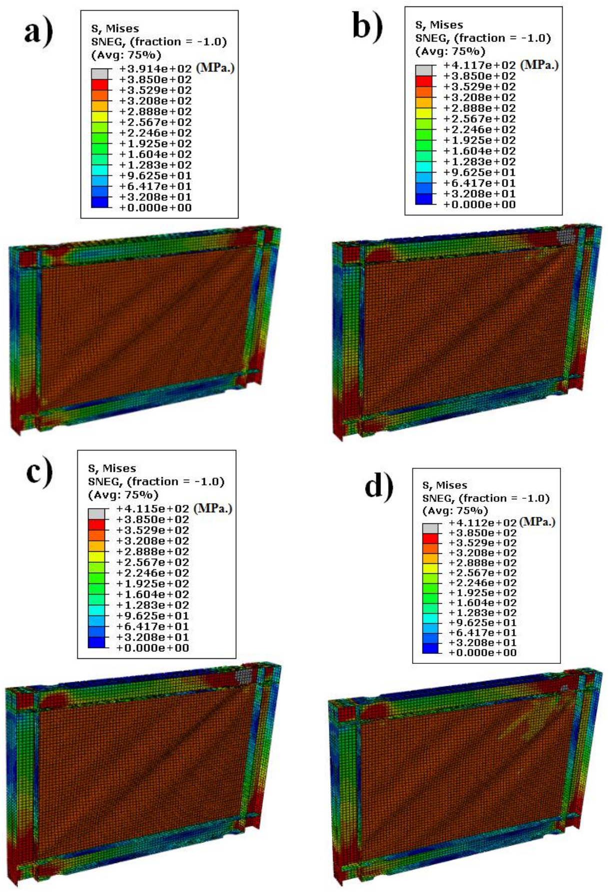

Fig. 6 Mises stress distributions in typical SPSWs (n = 1, L/h = 1.43) at the ultimate state: (a) unreinforced (S); and reinforced with, (b) CS ($\theta_f = 45°$); (c) CP ($\theta_f = 45°$); and (d) CD patterns

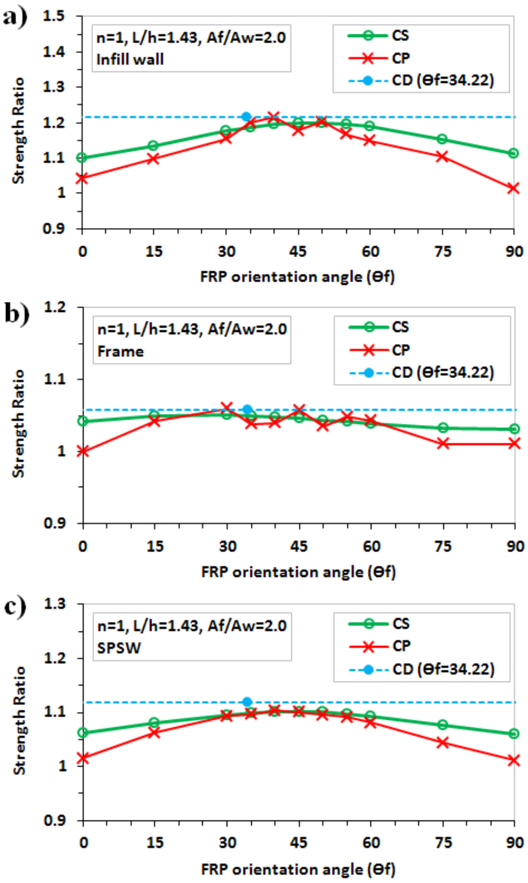

Fig. 7 Variations of the ultimate strength ratios of (a) infill walls; (b) frames; and (c) total systems with the orientation angle of FRP in typical CSPSWs (n = 1, L/h = 1.43, A_F/A_w = 2.0) for different reinforcement patterns

3.2 The effect of FRPs orientation (θ_f)

According to the literature (Hatami *et al*. 2012, Nateghi-Alahi and Khazaei-Poul 2012), the orientation angle of fibers can be an effective factor in the design and behavior of FRP-reinforced SPSWs. In this section, parametric studies are done to investigate the effects of fiber orientation on the nonlinear behavior of typical single-story SPSWs ($L/h = 1.43$) reinforced with the CP and CS patterns (unlike these two patterns, as mentioned before, the fiber orientation in an individual SPSW reinforced with the CD pattern is along the diagonal and constant; therefore, no parametric studies are done for this reinforcement pattern).

In the considered models, the orientation angle of θ_f (see Fig. 1) is assumed to vary from 0 (horizontal) to 90º (vertical). The strips are considered to have a width of $w_f = 350$ mm in both the CP and CD patterns. For comparison purposes, the fiber thicknesses (number of layers) in the different patterns are determined in a way that the fiber content is kept constant for all reinforcement patterns (i.e., $A_F/A_w \cong 2$).

3.2.1 Ultimate strength

Fig. 7 shows the effect of orientation angle of FRPs on the ratios of ultimate strengths of the reinforced-infill wall, frame, and total reinforced system for the CP and CS patterns for a typical single-story SPSW with an aspect ratio of $L/h = 1.43$. For comparison purposes, the results for the CD pattern (having a fixed orientation angle along the diagonal) are also shown in Fig. 7. The total strength of the reinforced-wall is obtained from that of the infill wall only (calculated by means of integrating shear stresses across the width of the infill wall) and that of fibers (from ABAQUS) at the lower level. The ultimate strength of the frame is determined by subtracting that of the reinforced-wall (infill wall + FRPs) from that of the total system. As can be seen, both of the infill wall and total system strength ratios for the CP and CS patterns are maximized at an orientation angle between 40 to 45° (almost close to the infill wall tension field angle). However, the changes in the orientation of FRPs do not result in significant changes in the frame strength ratio. Comparing the obtained results for these two patterns with the CD pattern in Fig. 7 (for a typical SPSW with $L/h = 1.43$) is shown that the CD pattern would be preferred over the other reinforcement patterns to increase the ultimate strength, if the optimal orientation angle of FRP is unknown.

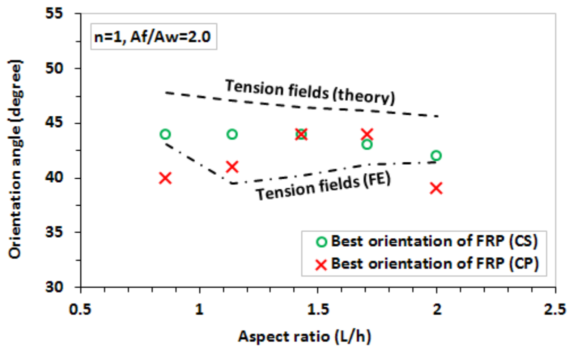

Fig. 8 Comparison of (average) angle of tension fields (from analysis and theory) and optimal orientation angle of FRP for CSPSWs (n = 1) of different aspect ratios and with reinforcement patterns of CP and CS

To further investigate the relation between the optimal orientation angle of FRP and tension field angle, Fig. 8 compares the optimal orientation angle of FRP (regarding the maximum strength) for the CP and CS patterns with the plate tension field angles obtained from the theory (AISC 341-05 2005) or ABAQUS, for typical SPSWs with different aspect ratios (all angles are expressed relative to horizontal axis). As can be seen in Fig. 8 and in agreement with the results of previous studies (Nateghi-Alahi and Khazaei-Poul 2012), there is a reasonable correlation between the plate tension field angle and optimal orientation angle of FRPs in the infill plate, regardless of the reinforcement pattern and aspect ratio of system. Based on the obtained results, the use of fibers with an orientation angle of 40 to 45° (relative to horizontal axis) will maximize the strength of different SPSWs.

3.2.2 Initial stiffness and ductility

Figs. 9-10 respectively show the ratios of initial stiffness and ductility of reinforced models to those of the

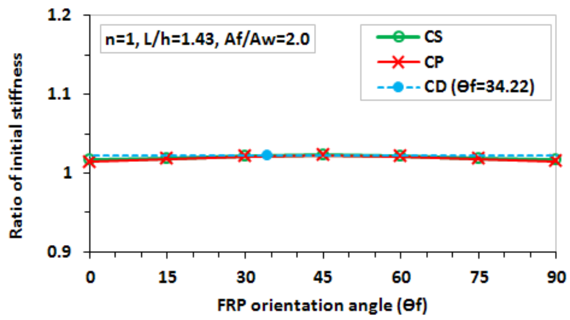

Fig. 9 Variations of the initial stiffness ratios with orientation angle of FRP in typical CSPSWs (n = 1, L/h = 1.43, A_F/A_w = 2.0)

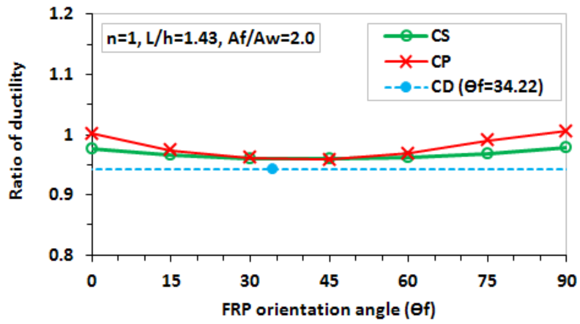

Fig. 10 Variations of the ductility ratios with orientation angle of FRP in typical CSPSWs (n = 1, L/h = 1.43, A_F/A_w = 2.0)

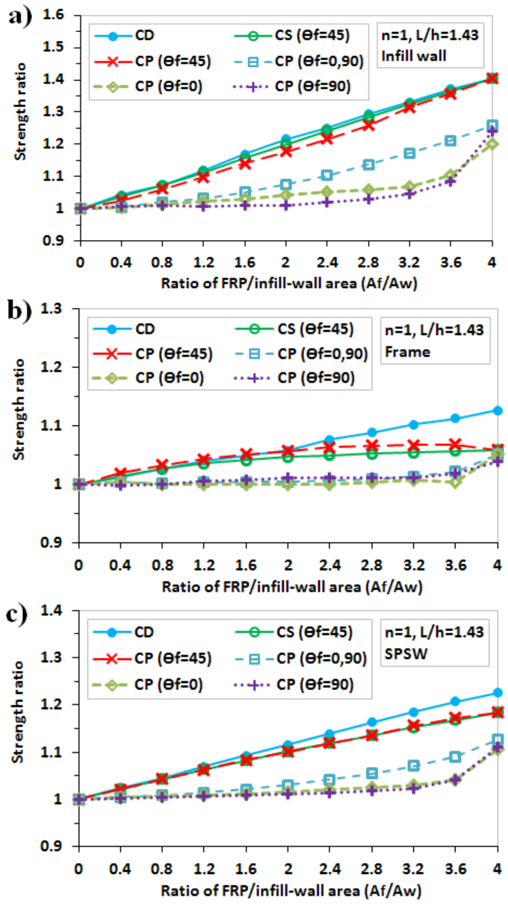

Fig. 11 Variations of the ultimate strength ratios of (a) infill wall; (b) frame; and (c) total system in typical CSPSWs having different ratios of A_F/A_w (fiber content)

corresponding unreinforced models as a function of the orientation of FRPs for the different reinforcement patterns. The initial stiffness is calculated by dividing the base shear by the roof displacement at the early stage of nonlinear analysis. The ductility was determined as the ratio of the maximum displacement to the yield displacement (i.e., $\mu = \delta_{max}/\delta_y$). The maximum displacement (δ_{max}) was defined as the top story displacement at the drift ratio of 2.5%. The yield displacement (δ_y) was calculated through the concept of equal plastic energy, so that the area surrounded by the idealized elasto-plastic curve was equal to that of the actual pushover curve (Hosseinzadeh and Tehranizadeh 2012).

As shown in Fig. 9, regardless of the reinforcement pattern and orientation angle of FRPs, the use of fibers has no significant effect on the initial stiffness of SPSWs, although it may have some effects on the stiffness during the loading as can be implied from the results in Fig. 5. Also, the results in Fig. 10 indicate that the use of fibers may adversely affect the ductility of SPSWs due to the delay in the initiation of yielding in the infill wall, although the effects for the considered cases in this section are not significant (about 5%).

3.3 The effect of FRP reinforcement content

In this section, the effect of fiber content (by changing the fiber width or number of layers so that $A_f/A_w = 0{\sim}4.0$) on the system behavior is investigated for typical single-story SPSWs ($L/h = 1.43$) strengthened with the different reinforcement patterns. In the considered models reinforced with the CP pattern, the width of strips (w_f) varies from 70 to 700 mm (i.e., $w_f/s_f = 0.1{\sim}1$); the orientation angles are considered to be 0 (horizontal), 90 (vertical), both 0 (horizontal on one side) and 90 (vertical on the other side of the infill plate) simultaneously, and 45°; while the total thickness of fibers is kept constant ($t_f = 2$ mm, equivalent to the use of two layers of FRP on each side of the infill plate). In the CD reinforcement pattern, the width of strips varies from 70 to 700 mm with the constant total thickness of $t_f = 8$ mm (equivalent to 8 layers on each side of the infill plate). In the CS reinforcement pattern, the orientation angle of FRPs equals 45°, while the total thickness of FRPs is considered to vary from 0.5 (one layer in one side of the infill plate) to 2 mm (2 layers on each side of the infill plate).

3.3.1 Ultimate strength

Fig. 11 shows the variations of ultimate strength ratios of the reinforced-wall, frame and total system for composite SPSWs to those of the corresponding unreinforced model ($L/h = 1.43$) against different FRP content (A_F/A_w). From the results in Fig. 11, the following points can be noted:

- The maximum strength for a reinforced single-story SPSW (especially at high fiber contents) can be achieved for the reinforcement patterns of CD and CS/CP (with an angle of 45°), respectively.
- In general, the use of fibers along directions other than those of the plate tension fields reduces the effectiveness of reinforcement.
- The use of fibers in both vertical and horizontal directions simultaneously is more effective than that only along the one of the horizontal and vertical directions.
- Due to the changes in the infill wall properties and the wall-frame interaction effect, the behavior of frame in a reinforced or unreinforced single-story SPSW is somewhat different. Similar results were obtained by previous research for the behavior of frames in SPSWs with different infill wall thicknesses (Habashi and Alinia 2010), or for the behavior of SPSW frame and the corresponding bare frame (Hosseinzadeh and Tehranizadeh 2014b).

3.3.2 Initial stiffness and ductility

Figs. 12-13 respectively compare the ratios of initial stiffness and ductility of reinforced SPSWs to those of the corresponding unreinforced SPSW ($L/h = 1.43$) for the considered reinforcement patterns.

As seen in Fig. 12, for all reinforcement patterns, the initial stiffness ratio of composite SPSWs increases linearly with the FRP content. However, the amount of increases in the initial stiffness is not considerable even at the highest fiber content (about 5% for $A_F/A_w = 4.0$).

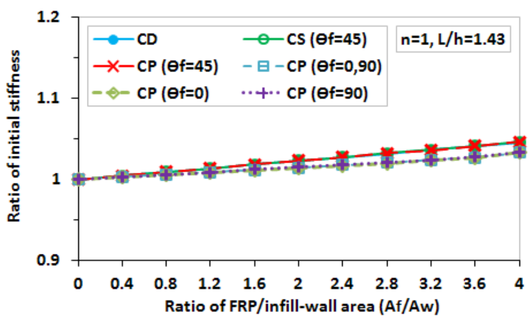

Fig. 12 Initial stiffness ratios of typical CSPSWs (*n* = 1, *L*/*h* = 1.43) for different ratios of A_F/A_w

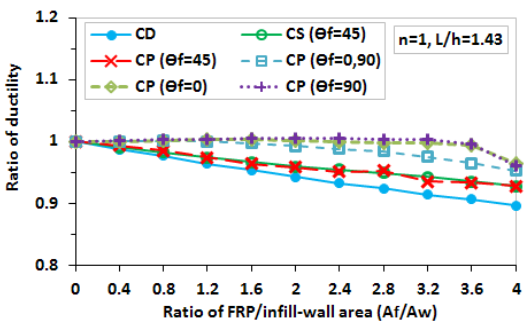

Fig. 13 Ductility ratios of typical CSPSWs (*n* = 1, *L*/*h* = 1.43) for different ratios of A_F/A_w

Similar to the results in Fig. 10, Fig. 13 also verifies that the use of FRPs for the reinforcement of SPSWs may adversely reduce the ductility of the system. This can be explained by the fact that the presence of FRPs delays the yielding in the infill wall, thereby reducing the ductility of the SPSW system which is mainly influenced by the nonlinear behavior of the infill plate (Hosseinzadeh and Tehranizadeh 2012). Likewise, the reductions in the ductility for the considered cases in this section are not significant, too. According to the obtained results, a maximum ductility reduction of about 10% is observed at $A_F/A_w = 4.0$ for the CD pattern.

Fig. 14 is utilized to assess the effect of further reinforcement (in particular, only by increasing the thickness or layers of reinforcement fibers) on the strength, stiffness and ductility of a typical SPSW ($L/h = 1.43$) for the considered reinforcement patterns. In the parametric studies, the thickness of fibers in the CP, CD and CS patterns ranges from 1-8, 4-32 and 0.5-4 mm respectively (i.e., $A_F/A_w = 0{\sim}8.0$), while the orientation angle of FRPs in the CP and CS patterns equals 45° ($\theta_f = 45^\circ$) and the width of strips in the CP and CD patterns is 350 mm ($w_f = 350$ mm).

As can be observed in Fig. 14(a), at relatively lower fiber contents (i.e., $A_F/A_w \leq 4$), the ultimate strength ratio

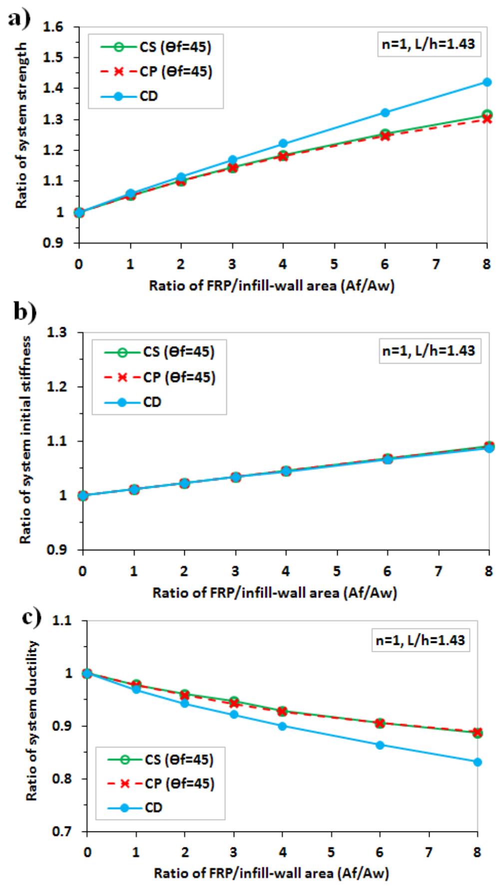

Fig. 14 Variations of a) ultimate strength; (b) initial stiffness; and (c) ductility ratios in typical CSPSWs (*n* = 1, *L*/*h* = 1.43) having different ratios of A_F/A_w (fiber content)

of the system for the all reinforcement patterns is almost the same and increases linearly with the fiber content (A_F/A_W). At higher fiber contents ($A_F/A_W > 4$), however, the effectiveness of the reinforcement with the CS or CP patterns is decreased and thus, the reinforcement with the CD pattern is preferred to the others to achieve higher strength. This reduction in the strength can be explained by the premature yielding or excessive deformation of frame members resulting from the additional loads imposed by the reinforced-wall. In the case of the CP or CS reinforcement patterns, the additional loads from fibers act along the frame members, thereby increasing all the axial, shear and flexural demands in frame members, while in the case of the CD pattern, the fibers impose forces on frame members through panel zones, thus increasing only the axial demand in frame members. As a result, the undesirable effects of the forces induced by fibers on frame members can be more pronounced for the reinforcement patterns of CS/CP than CD. This would be of great concern, especially where the SPSW frame is not stiff/strong enough to resist against the additional forces from the reinforced infill wall.

From the results in Figs. 14(b) and (c), regardless of the reinforcement pattern, a maximum increase of about 10% and a maximum reduction of about 15% (at fiber content of $A_F/A_W = 8.0$), respectively, in the initial stiffness and ductility of reinforced SPSWs are observed, as compared to those of the corresponding unreinforced SPSWs. Based on the results in Fig. 14(c), unlike the results in Fig. 14(a) for the strength, the maximum reduction in the ductility is observed for the CD pattern.

3.4 The effect of FRP type

In this section, the effect of fiber type (material) on the behavior of typical composite SPSWs ($L/h = 1.43$) is investigated for the considered reinforcement patterns. According to Table 3, in addition to the default reinforcement fiber (glass fiber of type G1), another type of glass fiber (type G2) and a type of carbon fiber (C) are also considered for the studies. In the considered models, regardless the fiber type, the total thicknesses of fibers in the CS, CP and CD patterns are assumed to be 1, 2 and 8 mm, respectively, so that the fiber content is the same for all the reinforcement patterns. Also, the orientation angle of fibers in the CS and CP patterns is considered equal to $\theta_f = 45^\circ$ to ensure the highest performance of SPSWs reinforced with these patterns.

Fig. 15 compares the behavior of SPSWs reinforced with the different fiber types (C, G1 and G2) and patterns (CS, CL and CD). Because of the relatively higher modulus of elasticity and longitudinal tensile strength of carbon fibers (see Table 3), the SPSW reinforced with the C-fibers, regardless of the reinforcement pattern, shows a higher

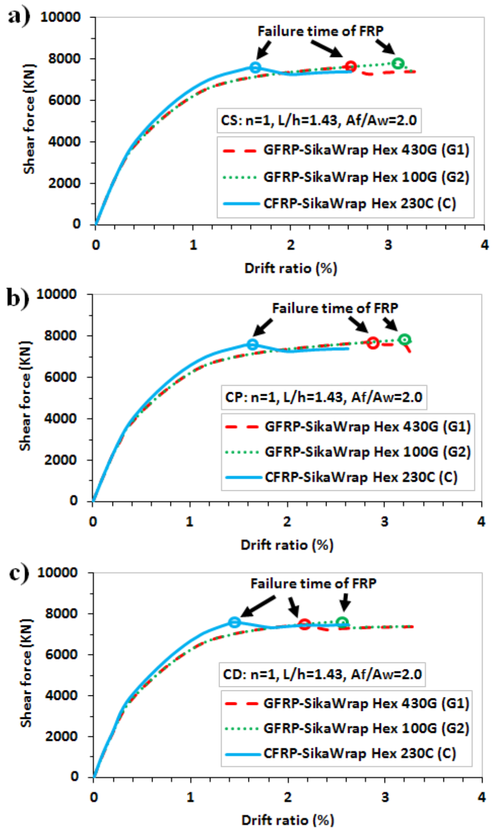

Fig. 15 Shear force–drift ratio curves of typical CSPSWs ($n = 1$, $L/h = 1.43$, $A_F/A_W = 2.0$) having different FRP types (G1, G2 and C) and with (a) CS; (b) CP; and (c) CD patterns

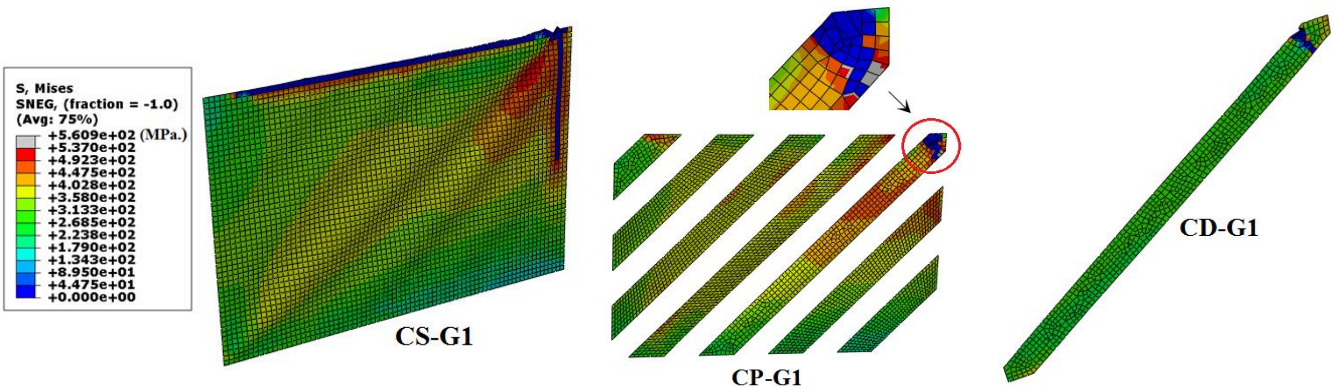

Fig. 16 Mises stress distributions and rupture patterns in the fiber laminates of typical CSPSWs ($n = 1$, $L/h = 1.43$, $A_F/A_W = 2.0$) having different reinforcement patterns (CS ($\theta_f = 45°$), CP ($\theta_f = 45°$) and CD)

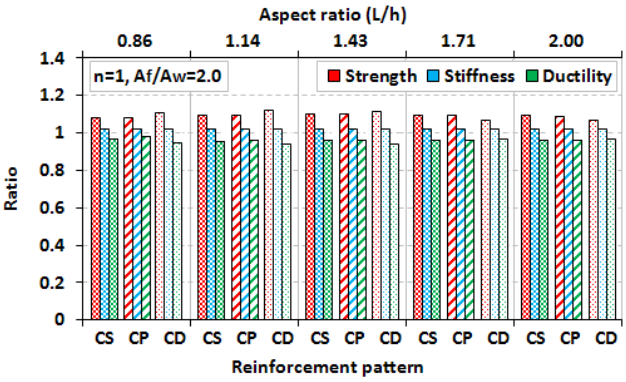

Fig. 17 Ratios of ultimate strength, initial stiffness and ductility for CSPSWs ($n = 1$, $A_F/A_w = 2.0$) having different reinforcement patterns and aspect ratios

strength than those reinforced with the G1- or G2-fibers, as expected. However, due to the smaller tensile elongation of the carbon fibers, as noted in Table 3, the rupture in the C-fibers occurs at a relatively lower drift ratio during loading. Moreover, no significant difference between the behaviors of different models reinforced with the G1- and G2-fibers, which have relatively different specifications but almost the same modulas of elsticity, is observed prior to fiber rupture. However, because of a higher tensile elongation, the rupture in the G2-fibers occurs later than G1-fibers in different reinforced models. Thus, it can be generally concluded that the ultimate strength of the FRP-reinforced system is principally affected by both the fiber modulus of elasticity and longitudinal tensile strength, while the occurrence of rupture in the fibers is mainly influenced by its ultimate tensile elongation (material ductility).

The von-Mises stress distributions in fibers of G1-type shown in Fig. 16 are utilized to specifically illustrate the typical behavior (rupture propagation patterns) of fibers in composite SPSWs having different reinforcement patterns at the failure stage. Fairy similar results are obtained for the C- and G2-fiber materials and thus, are not presented here for brevity. Indeed, the type of fiber material does not significantly affect the pattern of rupture in the fibers, despite its impact on the occurrence time of rupture (failure) as discussed above. In the CS pattern, the rupture initiates from the upper tensile corner of the fiber and extends longitudinally and transversely along the fiber interfaces with boundary frame members. In the CD pattern, the rupture initiates from the edge of fibers at the upper tensile corner and extends transversely perpendicular to the fiber orientation. In the CP pattern, the rupture in the fibers occurs only in one of the strips, while the others remain intact, as indicated in Fig. 16. The initiation and propagation of rupture in this strip are almost similar to that observed in the CD pattern.

In view of the discussions above (in regard to initiation and propagation of rupture), the reinforcement with the CP pattern may be preferred to the other patterns, since the growth of rupture in a certain strip is independent of the adjacent strips. This would limit the rupture propagation in the fibers.

3.5 The effect of system aspect ratio

The effectiveness of the considered reinforcement patterns in improving the behavior of single-story SPSWs having different aspect ratios ($L/h = 0.86$, 1.14, 1.43, 1.71 and 2.00) is studied in this section. In the considered models, the width of fiber strip in the CP and CD patterns is 350 mm ($w_f = 350\ mm$). The orientation of fiber in the CS and CP patterns is selected to be 45° to maximize the strength. The fiber thicknesses (number of layers) in the different reinforcement patterns are selected in such a way that the fiber content is kept the same in all the reinforcement patterns ($A_F/A_w = 2.0$).

Fig. 17 depicts the ultimate strength, initial stiffness and ductility ratios of reinforced SPSWs having different aspect ratios and reinforcement patterns. The results demonstrate that in general, the system aspect ratio is not an important factor in the behavior (strength, initial stiffness and ductility ratios) of fiber-reinforced SPSWs. However, from the results, a small reduction in the strength ratios of SPSWs reinforced with the CD pattern and having relatively high aspect ratios (i.e., $L/h = 1.71$ and 2.00) can be observed. This can be explained by the variation and inconsistency between the fiber strip orientation and tension fields in such SPSWs, which in turn reduce the effectiveness of the reinforcement. On the contrary, in SPSWs with lower aspect ratios (i.e., $L/h = 0.86$, 1.14 and 1.43) the systems reinforced with the CD pattern perform somewhat stronger than others.

3.6 The effect of system height

In addition to single-story models, the effectiveness of the considered reinforcement patters in improving the behavior of multi-story (up to 8 stories) SPSWs (with $L/h = 1.43$) is studied in this section. The following assumptions are made in the considered models. In the case of CP pattern: $w_f/s_f = 350/700 = 0.5$ and $\theta_f = 45^{\circ}$; in the case of CD pattern: $w_f = 350\ mm$, and in the case of CS pattern: $\theta_f = 45^{\circ}$. Also, the thickness (number of layers) of fibers for each reinforcement pattern is selected such that fiber content is almost the same in all patterns ($A_F/A_w = 2.0$).

Fig. 18 studies the effect of the three reinforcement patterns on the ultimate strength, initial stiffness and ductility ratios of single- to 8-story CSPSWs. The results in Fig. 18 confirm that in multi-story cases, unlike the single-story ones, reinforcing the SPSWs with the CP or CS patterns, in which the reinforcements are used in a larger/whole surface area of the infill wall, results in a slightly higher strength. However, the effectiveness of different reinforcement patterns generally decreases for taller (6 and 8-story) SPSWs, probably due to the dominance of the flexural deformation over the shear behavior.

Similar to the results in the previous sections, Fig. 18 does not show any significant change in the initial stiffness of single- and multi-story CSPSWs, as compared to that of the corresponding unreinforced SPSWs. Moreover, compared with the single-story model, fiber reinforcement

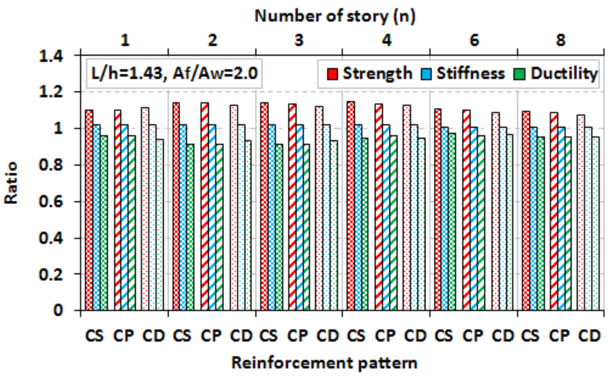

Fig. 18 Ratios of ultimate strength, initial stiffness and ductility for CSPSWs ($L/h = 1.43,\ A_F/A_w = 2.0$) having different reinforcement patterns and heights

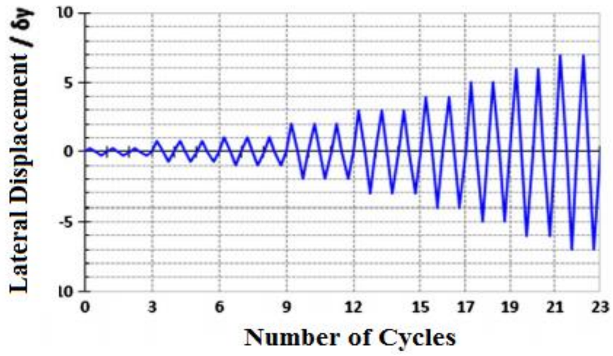

Fig. 19 Cyclic displacement history

may cause further reduction in the ductility ratio of multi-story SPSWs, as noted in Fig. 18 (up to about 10% for $A_F/A_w = 2.0$).

3.7 The effect of FRP reinforcement on the energy dissipation

To further investigate the effect of the reinforcement patterns on the behavior of SPSWs, the cyclic performance of typical single- and 4-story FRP-reinforced systems ($L/h = 1.43$) is studied and compared with those of the corresponding unreinforced models.

Given the cyclic nature of loading, the reinforced SPSWs are provided with two series of fibers oriented in both directions (the chosen fiber pattern is duplicated in a mirror image) so that the behaviors of CSPSWs remain symmetric in both sway directions. In each direction, the total thicknesses of fibers in the CP ($t_f = 2\,mm,\ w_f/s_f = 350/700 = 0.5,\ \theta_f = +45^{\circ}$ and -45°), CS ($t_f = 1\,mm,\ \theta_f = +45^{\circ}$ and -45°) and CD ($t_f = 8\,mm,\ w_f = 350$ mm, $\theta_f =$ along diagonal direction) patterns are selected in such a way that the fiber content is the same for all the reinforcement patterns ($A_F/A_w = 2.0$).

According to pushover analyses, the yield displacement (δy), which is the basic parameter in cyclic loading, for single- and four-story reinforced SPSWs was estimated to occur at roof displacements of 12.5 and 43 mm, respectively. For comparison purposes, a similar loading pattern is used for the reinforced SPSWs and their corresponding unreinforced models. According to ATC-24 guideline (ATC 1992), the cyclic loading is applied to the upper HBE at the roof level by applying a total of 23 cycles of displacement loading (up to a displacement of 7δy), as shown in Fig. 19.

Fig. 20 compares the hysteresis curves of the infill wall, frame and total system for the unreinforced and reinforced models considered in this section. In general, a relatively similar pattern is observed for the respective hysteresis curves of the infill wall, frame and total system in both the reinforced and unreinforced models. However, from the results, an improvement in the dissipated energy (surrounded surface area by the hysteresis loop) of the infill

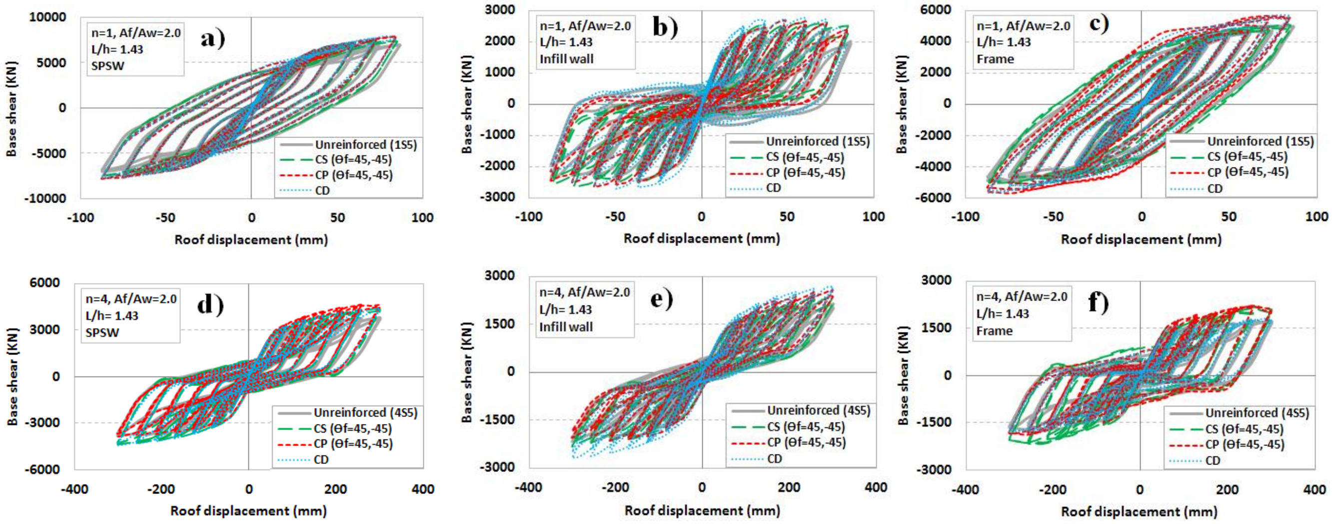

Fig. 20 Hysteresis curves for typical SPSWs and CSPSWs (n = 1 and 4, L/h = 1.43, $A_F/A_w = 2.0$) with different reinforcement patterns (CS, CP and CD): (a) SPSW (n = 1); (b) infill wall (n = 1); (c) frame (n = 1); (d) SPSW (n = 4); (e) infill wall (n = 4); and (f) frame (n = 4)

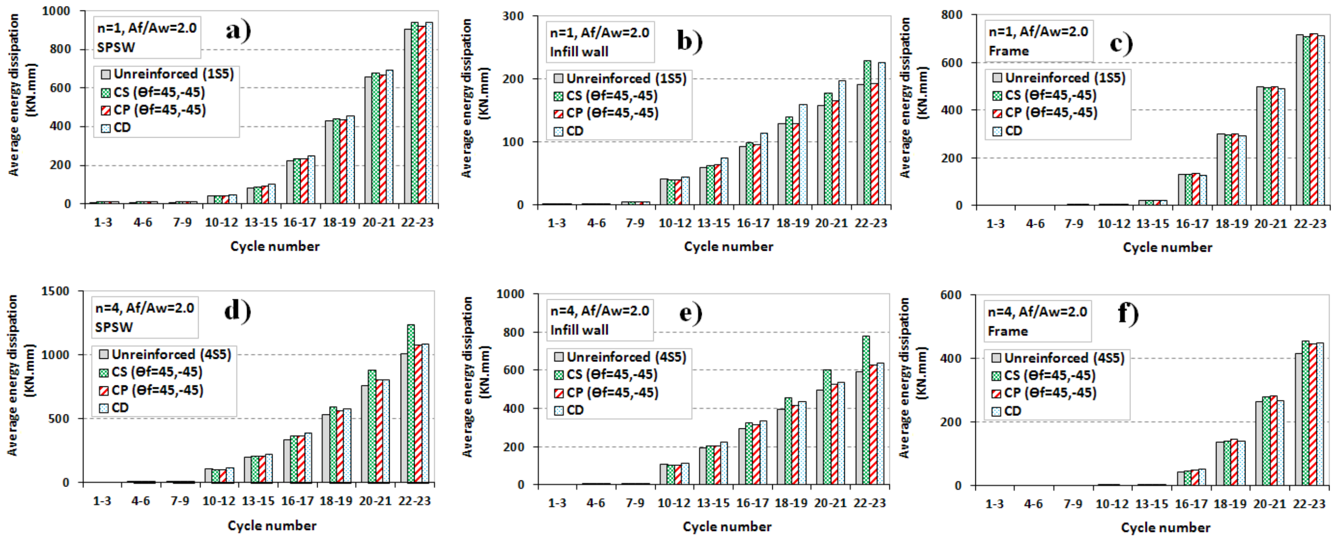

Fig. 21 Average energy dissipations in the different cycles for typical SPSWs and CSPSWs (n = 1 and 4, L/h = 1.43, $A_f/A_w = 2.0$) with different reinforcement patterns (CS, CP and CD): (a) SPSW (n = 1); (b) infill wall (n = 1); (c) frame (n = 1); (d) SPSW (n = 4); (e) infill wall (n = 4); and (f) frame (n = 4)

wall (and therefore, the total system) in reinforced SPSWs compared to that of the unreinforced ones is evident. This is mainly due to the increase in the strength of the reinforced wall rather than due to the changes in the pinching phenomenon effects in the reinforced and unreinforced systems. In other words, the use of fibers in a SPSW has no significant effect on the pinching phenomenon and the corresponding reduction of energy in the system. The results also show that the energy dissipation capacity of frame, especially in 4-story cases, changes to some extent, due to the change in the properties of infill wall and its interactive behavior with frame.

Fig. 21 quantitatively compares the energy dissipation characteristics of unreinforced and reinforced single- and 4-story SPSWs in different loading cycles for various reinforcement patterns. Energy dissipation, as a major seismic characteristic, is calculated by the surface area surrounded by the hysteresis curves during each loading cycle. As mentioned before, the energy dissipation capacity of the infill wall and therefore, the total system is improved by using fibers on both sides of the infill wall. From the point of view of maximum energy dissipation capacity, in the case of single-story SPSWs that the shear deformation is dominant, the system behavior for all the reinforcement patterns is somewhat similar, while in the case of 4-story systems that the flexural deformation effects become more significant, the SPSW reinforced with the CS pattern performs distinctly better than others, especially in the cycles with large deflections.

4. Estimating the strength of FRP-reinforced SPSWs with RBS connections

The total strength of a reinforced SPSW (F_{CSW}) can be determined from Eq. (1), based on the frame strength (F_{frame}), infill wall strength (F_{wall}) and fiber strength (F_{FRP}).

$$\mathrm{F_{CSW}} = \mathrm{F_{wall}} + \mathrm{F_{frame}} + \mathrm{F_{FRP}} \tag{1}$$

The infill wall strength (F_{wall}) is obtained from Eq. (2).

$$\mathrm{F_{wall}} = \mathrm{C_P} \times \left[0.5 \times \mathrm{F_{yw}} \times \mathrm{b_w} \times \mathrm{t_w} \times \sin(2\alpha)\right] \tag{2}$$

Where C_P is correction factor for the infill wall strength determined based on the development of yielding in the infill wall, the difference in the nominal and expected yield stresses of the infill wall and the changes in the infill wall tension field angle as a result of the wall-frame interaction (where the frame members are strong and stiff enough, as for the considered systems in this study, $C_P \cong 1$); t_w, b_w and F_{yw} respectively represent thickness, width and yield stress of the infill wall; and α shows the plate tension field angle (relative to the vertical axis), calculated from Eq. (3) (AISC 341-05 2005)

$$\tan^4(\alpha) = \frac{1 + \left(\frac{\mathrm{t_w\,L}}{2\mathrm{A_c}}\right)}{1 + \mathrm{t_w h}\left(\frac{1}{\mathrm{A_b}} + \frac{\mathrm{h^3}}{360\mathrm{I_c\,L}}\right)} \tag{3}$$

Where A_b is HBE section area; A_c and I_c are the VBE section area and moment of inertia, respectively; and L and h are respectively the system width and height.

The frame strength (F_{frame}) is calculated from Eq. (4) assuming formation of plastic hinges at the bases of VBEs and both ends of HBEs.

$$\mathrm{F_{frame}} = \mathrm{C_F} \times \left[\frac{2 \times (\mathrm{M_{Pc}} + \lambda \times \mathrm{M_{Pb}})}{\mathrm{h}}\right] \tag{4}$$

Where λ is the ratio of center-to-center distance of VBEs to the center-to-center distance of RBS connections at HBE ends; M_{Pb} and M_{Pc} respectively show the plastic moment capacities of HBEs and VBEs; and C_F is the correction factor for the frame strength, considering the effect of wall-frame interaction and the difference between expected and nominal yield stress of frame materials. A correction factor of $C_F = 1{\sim}1.2$ was obtained from analyzing different SPSW models (an average value of $C_F = 1.1$ would be considered).

Finally, the strength of FRPs (F_{FRP}) is determined as follows according to the reinforcement pattern:

a. CD pattern:

The strength of FRPs with the CD pattern ($F_{FRP(CD)}$) is calculated from Eqs. (5)-(8)

$$\begin{aligned} F_{FRP(CD)} = {} & C_e \times [0.5 \times \sigma_{1.FRP} \times (w_f / \sin\theta_f) \times t_f \times \sin 2\alpha] \\ & + C_p \times [\sigma_{2.FRP} \times w_f \times t_f \times \cos\theta_f] \end{aligned} \tag{5}$$

$$\sigma_{1.FRP} = \frac{E_{xf}}{\beta . E_{sw}} F_{yw} \tag{6}$$

$$\sigma_{2.FRP} = E_{xf} \times \varepsilon_{FRP} \leq T_x \tag{7}$$

$$\begin{aligned} \varepsilon_{FRP} = {} & \left[\sqrt{\left(b_w + U - U_{cy}\right)^2 + {d_w}^2} - \sqrt{{b_w}^2 + {d_w}^2}\right] \\ & \div \sqrt{{b_w}^2 + {d_w}^2} \end{aligned} \tag{8}$$

Where, C_e is a correction factor for the portion of fiber strength before occurrence of yielding in the infill wall (elastic stage). This correction factor can be dependent on different factors such as column rigidity, type of beam-column connection (Khazaei-Poul and Nateghi-Alahi 2012) and geometrical properties of the system and fibers. According to the results obtained from analyses for the reinforcement pattern of CD, C_e in the models under study varies from 0.5 to 0.7 (on average, a value of $C_e = 0.6$ would be considered); $\sigma_{1.FRP}$ is the tensile stress of fibers at the yield of composite wall; E_{sw} is the modulus of elasticity of the infill wall; β is a coefficient in the relationship between the strain of fiber laminates and infill wall. In the case of full adhesion between the surface of the infill wall and fiber laminates (as assumed in this study), it equals unity, $\beta = 1$ (Khazaei-Poul and Nateghi-Alahi 2012); $\sigma_{2.FRP}$ is the maximum longitudinal tensile stress tolerated by fibers at the ultimate state (or at the time of fiber rupture) and is determined by multiplying the longitudinal strain of fibers (ε_{FRP}) by its longitudinal tensile modulus of elasticity (E_{xf}), considering the elastic behavior of fibers during loading. Note that $\sigma_{2.FRP}$ is limited to the fiber tensile strength, T_x. Taking into account the effect of shear deformations in the system, the longitudinal strain of fibers (ε_{FRP}) at the ultimate state is obtained from Eq. (8) (According to Fig. 22). The effect of transverse strain, compared to the longitudinal strain, is neglected in this equation; U_{cy} represents the limiting elastic shear displacement of the composite wall which is determined by solving Eq. (9).

$$\varepsilon_{yw} = \frac{F_{yw}}{E_{sw}} = \frac{\sqrt{\left(b_w + U_{cy}\right)^2 + {d_w}^2} - \sqrt{{b_w}^2 + {d_w}^2}}{\sqrt{{b_w}^2 + {d_w}^2}} \tag{9}$$

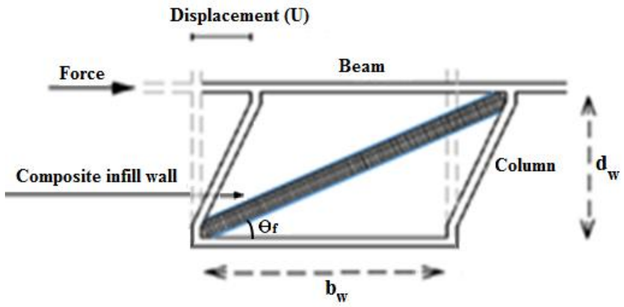

Fig. 22 Behavior of CSPSWs with the CD reinforcement pattern

Where, d_w is depth of infill wall, and ε_{yw} is the strain of the composite wall at the diagonal yield of the infill wall; U is the lateral story drift of the reinforced SPSW; C_p is a correction factor for determining the portion of fiber strength after ocurrence of yielding in the infill wall up to ultimate state and differs depending on the characteristics of diagonal fibers and wall. According to the analysis results of the models in this study, Eq. (10) is suggested for estimation of C_p.

$$C_p = 0.25 \times (L/h) + 0.30 \tag{10}$$

b. CS pattern:

According to Ref. (Khazaei-Poul and Nateghi-Alahi 2012), the strength of fibers with the CS pattern (in optimal direction, along the infill wall tension fields) is calculated from Eqs. (11) and (12)

$$\begin{aligned} F_{FRP(CS)} = {} & C_e \times [0.5 \times \sigma_{1.FRP} \times b_w \times t_f \times \sin 2\alpha] \\ & + C_p \times \left[\frac{E_{xf} \times b_w \times t_f \times (\sin 2\alpha)^2}{4 d_w}\right] \\ & \times \left(U - U_{cy}\right) \end{aligned} \tag{11}$$

$$U_{cy} = C_y \times \left(\frac{2F_{yw} \times d_w}{E_{sw} \times \sin 2\alpha}\right) \times \left(\frac{t_w + \frac{E_{xf} \times t_f}{2\beta^2 \times E_{sw}}}{t_w + \frac{E_{xf} \times t_f}{\beta^2 \times E_{sw}}}\right) \tag{12}$$

The correction factor of C_e can vary from 0.8 to unity for the CS pattern (Khazaei-Poul and Nateghi-Alahi 2012). Based on the analysis results for the models in this study, an average value of $C_e = 0.9$ seems to be appropriate.

The correction factor of C_p varies from 0.5 to 0.7 in this study. Based on the analysis results for the SPSW models, an average value of $C_p = 0.6$ can be considered.

The correction factor of C_y for yield displacement of the reinforced wall varies from 1 to 1.7. A value of $C_y = 1.65$ is considered for the models under study (Khazaei-Poul and Nateghi-Alahi 2012).

c. CP pattern:

To determine the strength of FRPs in the CP pattern ($F_{FRP(CP)}$), a correction factor defined as the ratio of the width of fiber strips to their center-to-center distance (w_f/s_f) is multiplied by the strength determined from Eq.

Table 7 Comparisons of the results of the strength calculated from the presented procedures with the FE analysis results for some CSPSW systems

Specifications of CSPSW	F_{FRP} (KN)		F_{wall} (KN)		F_{Frame} (KN)		F_{CSW} (KN)	
	Eqs. (5), (11) or (13)	FE	Eq. (2)	FE	Eq. (4)	FE	Eq. (1)	FE
CD, (n = 1, L/h = 0.86, A_F/A_w = 2)	258	278	1363	1425	3465	3488	5086	5191
CD, (n = 1, L/h = 1.14, A_F/A_w = 2)	398	403	1882	1976	3676	3846	5956	6225
CD, (n = 1, L/h = 1.43, A_F/A_w = 2)	523	502	2400	2520	4418	4634	7341	7656
CD, (n = 1, L/h = 1.71, A_F/A_w = 2)	595	561	2914	3046	6207	6621	9716	10228
CD, (n = 1, L/h = 2.00, A_F/A_w = 2)	611	600	3429	3567	8391	9064	12431	13231
CS, (n = 1, L/h = 0.86, θ_f = 45, A_F/A_w = 2)	303	309	1363	1375	3465	3386	5131	5070
CS, (n = 1, L/h = 1.14, θ_f = 45, A_F/A_w = 2)	393	402	1882	1931	3676	3769	5951	6102
CS, (n = 1, L/h = 1.43, θ_f = 45, A_F/A_w = 2)	503	492	2400	2487	4418	4583	7321	7562
CS, (n = 1, L/h = 1.71, θ_f = 45, A_F/A_w = 2)	759	738	2914	3036	6207	6707	9880	10481
CS, (n = 1, L/h = 2.00, θ_f = 45, A_F/A_w = 2)	901	891	3429	3549	8391	9148	12721	13588
CP, (n = 1, L/h = 0.86, θ_f = 45, A_F/A_w = 2)	246	237	1363	1398	3465	3440	5074	5075
CP, (n = 1, L/h = 1.14, θ_f = 45, A_F/A_w = 2)	395	404	1882	1941	3676	3749	5953	6094
CP, (n = 1, L/h = 1.43, θ_f = 45, A_F/A_w = 2)	435	439	2400	2486	4418	4631	7253	7556
CP, (n = 1, L/h = 1.71, θ_f = 45, A_F/A_w = 2)	715	730	2914	3049	6207	6692	9836	10471
CP, (n = 1, L/h = 2.00, θ_f = 45, A_F/A_w = 2)	793	785	3429	3574	8391	9194	12613	13553

(11), as shown in Eq. (13).

$$F_{FRP(CP)} = (w_f/s_f) \times F_{FRP(CS)} \tag{13}$$

To validate the accuracy of the above equations, Table 7 compares the strength values of some reinforced SPSWs obtained from the above procedures and numerical analyses. As noted, good agreement between the results of numerical analyses and above equations is observed.

5. Conclusions

In this study, the effectiveness of three different reinforcement patterns of FRP (including single-strip (CD pattern), multi-strip (CP pattern) and fully (CS pattern) FRP strengthened models) on the improvement of the behavior of CSPSWs was investigated using the FEM. The effects of orientation, width, thickness and type (glass or carbon) of FRP sheets as well as the system aspect ratio and height on the behavior and energy dissipation of SPSWs were also considered. The obtained results showed that:

- In a SPSW system, the strength of the infill wall and therefore, the total system is increased using the fiber laminates, depending on the type/pattern/content of reinforcement. The strength of the frame also changes slightly, due to the change in the properties of the infill wall and its interactive behavior with the frame.
- Compared to unreinforced SPSWs, ductility of CSPSWs is decreased, due to the delay in the initiation of yielding in the infill wall, while their initial stiffness does not change significantly.
- In single-story SPSWs where the use of high reinforcement content is necessary and frame members is not stiff/strong enough, the reinforcement with the CD pattern would be preferred, since this pattern can cause a lower force demand in frame members compared to the other reinforcement patterns. In multi-story cases, unlike the single-story ones, reinforcing the SPSWs with the CP or CS patterns, in which the reinforcements are used in a larger/whole surface area of the infill wall, results in a slightly higher strength. However, the effectiveness of different reinforcement patterns generally decreases for taller SPSWs, probably due to the dominance of the flexural deformation over the shear behavior.
- In the case of CS and CP reinforcement patterns, the use of FPR sheets almost along the direction of the infill wall tension fields can maximize the effectiveness (strength) of reinforcement.
- In general, the system aspect ratio is not an important factor in the behavior (strength, initial stiffness and ductility ratios) of fiber-reinforced SPSWs. However, a small reduction in the strength ratios of SPSWs reinforced with the CD pattern and having relatively high aspect ratios was observed from the results. This can be explained by the variation and inconsistency between the fiber strip orientation and tension fields in such SPSWs, which in turn reduce the effectiveness of the reinforcement.
- The type/pattern/content of fibers does affect the nonlinear behavior and failure mode as well as the fiber rupture propagation pattern. In this regard, the system strength is principally affected by both the fiber modulus of elasticity and longitudinal tensile

strength, while the occurrence of rupture in the fibers is mainly influenced by its ultimate tensile elongation (material ductility).

- The energy dissipation capacity of the infill wall and therefore, the SPSW system, can be improved using the fibers. In turn, the improvement is mainly due to the increase in the strength of the reinforced-wall rather than due to the changes in the pinching phenomenon effects.
- The strength of partially reinforced SPSWs can be estimated with reasonable accuracy using the proposed procedures for different reinforcement patterns.

References

ABAQUS (2014), Standard theory manual, Version 6.14-2, Hibbitt, Karlsson and Sorensen Inc., (HKS), USA.

AISC, ANSI/AISC 358-05 (2005), Prequalified connections for special and intermediate steel moment frames for seismic applications, American Institute of Steel Construction; Chicago, IL, USA.

AISC, ANSI/AISC 341-05 (2005), Seismic provisions for structural steel buildings, American Institute of Steel Construction; Chicago, IL, USA.

AISC, Steel Design Guide 20 (2007), Steel plate shear walls, American Institute of Steel Construction; Chicago, IL, USA.

Ali, M.M., Osman, S.A., Husam, O.A. and Al-Zand, A.W. (2018), “Numerical study of the cyclic behavior of steel plate shear wall systems (SPSWs) with differently shaped openings”, *Steel Compos. Struct., Int. J.*, **26**(3), 361-373. https://doi.org/10.12989/scs.2018.26.3.361

ASCE (2005), SEI/ASCE 7-05, Minimum design loads for buildings and other structures, American Society of Civil Engineers; VA, USA.

ATC (1992), Guidelines for cyclic seismic testing of components of steel structures for buildings, Report No. ATC-24, Applied Technology Council; Redwood City, CA, USA.

Bagherinejad, M.H. and Haghollahi, A. (2018), “Topology optimization of steel plate shear walls in the moment frames”, *Steel Compos. Struct., Int. J.*, **29**(6), 771-783. https://doi.org/10.12989/scs.2018.29.6.771

Barua, K. and Bhowmick, A.K. (2019), “Nonlinear seismic performance of code designed perforated steel plate shear walls”, *Steel Compos. Struct., Int. J.*, **31**(1), 85-98. http://dx.doi.org/10.12989/scs.2019.31.1.085

Brando, G. and De Matteis, G. (2011), “Experimental and numerical analysis of a multi-stiffened pure aluminium shear panel”, *Thin-Wall. Struct.*, **49**(10), 1277-1287. https://doi.org/10.1016/j.tws.2011.05.007

Chatterjee, A.K., Bhowmick, A. and Bagchi, A. (2015), “Development of a simplified equivalent braced frame model for steel plate shear wall systems”, *Steel Compos. Struct., Int. J.*, **18**(3), 711-737. https://doi.org/10.12989/scs.2015.18.3.711

Dakhel, M., Donchev, T. and Hadavinia, H. (2019), “Behaviour of connections for hybrid FRP/steel shear walls”, *Thin-Wall. Struct.*, **134**, 52-60. https://doi.org/10.1016/j.tws.2018.10.008

Deng, E.F., Zong, L. and Ding, Y. (2019), “Numerical and analytical study on initial stiffness of corrugated steel plate shear walls in modular construction”, *Steel Compos. Struct., Int. J.*, **32**(3), 347-359. https://doi.org/10.12989/scs.2019.32.3.347

Dhar, M.M. and Bhowmick, A.K. (2016), “Seismic response estimation of steel plate shear walls using nonlinear static methods”, *Steel Compos. Struct., Int. J.*, **20**(4), 777-799. https://doi.org/10.12989/scs.2016.20.4.777

Driver, R.G., Kulak, G.L., Kennedy, D.J.L. and Elwi, A.E. (1998), “Cyclic test of four-story steel plate shear wall”, *J. Struct. Eng.*, **124**(2), 112-120. https://doi.org/10.1061/(ASCE)0733-9445(1998)124:2(112)

Farzampour, A., Mansouri, I. and Hu, J.W. (2018), “Seismic behavior investigation of the corrugated steel shear walls considering variations of corrugation geometrical characteristics”, *Int. J. Steel Struct.*, **18**(4), 1297-1305. https://doi.org/10.1007/s13296-018-0121-z

Habashi, H.R. and Alinia, M.M. (2010), “Characteristics of the wall-frame interaction in steel plate shear walls”, *J. Constr. Steel Res.*, **66**(2), 150-158. https://doi.org/10.1016/j.jcsr.2009.09.004

Hatami, F., Ghamari, A. and Rahai, A. (2012), “Investigating the properties of steel shear walls reinforced with Carbon Fiber Polymers (CFRP)”, *J. Constr. Steel Res.*, **70**, 36-42. https://doi.org/10.1016/j.jcsr.2011.07.010

Hatami, F., Ghamari, A. and Hatami, F. (2014), “Effect of fiber angle on LYP steel shear walls behavior”, *J. Central South Univ.*, **21**(2), 768-774. https://doi.org/10.1007/s11771-014-2000-x

Hosseinzadeh, S.A.A. and Tehranizadeh, M. (2012), “Introduction of stiffened large rectangular openings in steel plate shear walls”, *J. Constr. Steel Res.*, **77**, 180-192. https://doi.org/10.1016/j.jcsr.2012.05.010

Hosseinzadeh, S.A.A. and Tehranizadeh, M. (2014a), “Behavioral characteristics of code designed steel plate shear wall systems”, *J. Constr. Steel Res.*, **99**, 72-84. https://doi.org/10.1016/j.jcsr.2014.04.004

Hosseinzadeh, S.A.A. and Tehranizadeh, M. (2014b), “The wall–frame interaction effect in steel plate shear wall systems”, *J. Constr. Steel Res.*, **98**, 88-99. https://doi.org/10.1016/j.jcsr.2014.02.013

Kalali, H., Hajsadeghi, M., Zirakian, T. and Alaee, F.J. (2015), “Hysteretic performance of SPSWs with trapezoidally horizontal corrugated web-plates”, *Steel Compos. Struct., Int. J.*, **19**(2), 277-292. https://doi.org/10.12989/scs.2015.19.2.277

Khazaei-Poul, M. and Nateghi-Alahi, F. (2012), “Theoretical and numerical study on the strengthened steel plate shear walls by FRP laminates”, *Int. J. Eng.*, **25** (1), 25-37.

Khazaei-Poul, M. and Nateghi-Alahi, F. and Zhao, X.L. (2016), “Experimental testing on CFRP strengthened thin steel plates under shear loading”, *Thin-Wall. Struct.*, **109**, 217-226. https://doi.org/10.1016/j.tws.2016.09.026

Kim, J., Kwon, M., Seo, H. and Jung, W. (2015), “Performance evaluation of GIP wall systems for strengthening steel-frame structures”, *Compos. Struct.*, **125**, 228-238. https://doi.org/10.1016/j.compstruct.2015.02.021

Kwon, M., Kim, J., Jung, W. and Seo, H. (2015), “Design procedure of GFRP-infill panels to improve the strength of steel-frame structures”, *Compos. Struct.*, **120**, 262-274. https://doi.org/10.1016/j.compstruct.2014.09.067

Liu, W.Y., Li, G.Q. and Jiang, J. (2018), ”Capacity design of boundary elements of beam-connected buckling restrained steel plate shear wall”, *Steel Compos. Struct., Int. J.*, **29**(2), 231-242. https://doi.org/10.12989/scs.2018.29.2.231

Lubell, A.S., Prion, H.G., Ventura, C.E. and Rezai, M. (2000), “Unstiffened steel plate shear wall performance under cyclic loading”, *J. Struct. Eng.*, **126**(4), 453-460. https://doi.org/10.1061/(ASCE)0733-9445(2000)126:4(453)

Massumi, A., Karimi, N. and Ahmadi, M. (2018), “Effects of openings geometry and relative area on seismic performance of steel shear walls”, *Steel Compos. Struct., Int. J.*, **28**(5), 617-628. https://doi.org/10.12989/scs.2018.28.5.617

Memarzadeh, P., Azhari, M. and Saadatpour, M.M. (2010), “A parametric study on buckling loads and tension field stress patterns of steel plate shear walls concerning buckling modes", *Steel Compos. Struct., Int. J.*, **10**(1), 87-108. https://doi.org/10.12989/scs.2010.10.1.087

Nateghi-Alahi, F. and Khazaei-Poul, M. (2012), "Experimental study of steel plate shear walls with infill plates strengthened by GFRP laminates", *J. Constr. Steel Res.*, **78**, 159-172. https://doi.org/10.1016/j.jcsr.2012.07.002

Petkune, N., Donchev, T., Hadavinia, H., Limbachiya, M. and Wertheim, D. (2016), "Performance of pristine and retrofitted hybrid steel/fibre reinforced polymer composite shear walls", *J. Constr. Build. Mater.*, **117**, 198-208. https://doi.org/10.1016/j.conbuildmat.2016.05.013

Petkune, N., Donchev, T., Hadavinia, H., Wertheim, D. and Limbachiya, M. (2018), "Comparison of the behavior of steel, pure FRP and hybrid shear walls under cyclic seismic loading in aspect of stiffness degradation and energy absorption", *J. Constr. Build. Mater.*, **165**, 621-630. https://doi.org/10.1016/j.conbuildmat.2017.12.013

Rahmzadeh, A., Ghassemieh, M., Park, Y. and Abolmaali, A. (2016), "Effect of stiffeners on steel plate shear wall systems", *Steel Compos. Struct., Int. J.*, **20**(3), 545-569. http://dx.doi.org/10.12989/scs.2016.20.3.545

Sahebjam, A. and Showkati, H. (2016), "Experimental study on the cyclic behavior of perforated CFRP strengthened steel shear walls", *Archives. Civil. Mech. Eng.*, **16**(3), 365-379. https://doi.org/10.1016/j.acme.2016.01.009

Shekastehband, B., Azaraxsh, A.A. and Showkati, H. (2017), "Hysteretic behavior of perforated steel plate shear walls with beam-only connected infill plates", *Steel Compos. Struct., Int. J.*, **25**(4), 505-521. https://doi.org/10.12989/scs.2017.25.4.505

Tabrizi, M.A. and Rahai, A. (2011), "Perforated steel shear walls with FRP reinforcement of opening edges", *Austral. J. Basic. Appl. Sci.*, **5**(10), 672-684.

Vatansever, C. and Berman, J.W. (2015), "Analytical investigation of thin steel plate shear walls with screwed infill plate", *Steel Compos. Struct., Int. J.*, **19**(5), 1145-1165. http://dx.doi.org/10.12989/scs.2015.19.5.1145

Vatansever, C. and Yardimci, N. (2011), "Experimental investigation of thin steel plate shear walls with different infill-to-boundary frame connections", *Steel Compos. Struct., Int. J.*, **11**(3), 251-271. http://dx.doi.org/10.12989/scs.2011.11.3.251

CC